



Chinese Pharmaceutical Association
Institute of Materia Medica, Chinese Academy of Medical Sciences

Acta Pharmaceutica Sinica B

www.elsevier.com/locate/apsb
www.sciencedirect.com



ORIGINAL ARTICLE

Purpurolide C-based microneedle promotes macrophage-mediated diabetic wound healing via inhibiting TLR4-MD2 dimerization and MYD88 phosphorylation



Yitong Liu^{a,b,†}, Guiyang Xia^{c,†}, Yingyi Chen^{a,b}, Huan Xia^c,
Junji Xu^{a,b}, Lijia Guo^{d,*}, Sheng Lin^{c,*}, Yi Liu^{a,b,*}

^aLaboratory of Tissue Regeneration and Immunology and Department of Periodontics, Beijing Key Laboratory of Tooth Regeneration and Function Reconstruction, School of Stomatology, Capital Medical University, Beijing 100050, China

^bImmunology Research Center for Oral and Systemic Health, Beijing Friendship Hospital, Capital Medical University, Beijing 100050, China

^cKey Laboratory of Chinese Internal Medicine of Ministry of Education and Beijing, Dongzhimen Hospital, Beijing University of Chinese Medicine, Beijing 100700, China

^dDepartment of Orthodontics, School of Stomatology, Capital Medical University, Beijing 100050, China

Received 2 April 2023; received in revised form 23 May 2023; accepted 24 May 2023

KEY WORDS

Diabetes;
Wound healing;
Purpurolide C;
Liposome and GelMA-
based microneedle
patches;
Macrophage polarization;

Abstract Delayed wound healing in diabetes is a global challenge, and the development of related drugs is a clinical problem to be solved. In this study, purpurolide C (PC), a small-molecule secondary metabolite of the endophytic fungus *Penicillium purpurogenum*, was found to promote diabetic wound healing. To investigate the key regulation targets of PC, *in vitro* RNA-seq, molecular docking calculations, TLR4-MD2 dimerization SDS-PAGE detection, and surface plasmon resonance (SPR) were performed, indicating that PC inhibited inflammatory macrophage activation by inhibiting both TLR4-MD2 dimerization and MYD88 phosphorylation. *Tlr4* knockout *in vivo* attenuated the promotion effect of PC on wound healing. Furthermore, a delivery system consisting of macrophage liposome and GelMA-

*Corresponding authors.

E-mail addresses: guolijia@mail.ccmu.edu.cn (Lijia Guo), lszn@bcm.edu.cn (Sheng Lin), lililiuyi@163.com (Yi Liu).

†These authors made equal contributions to this work.

Peer review under responsibility of Chinese Pharmaceutical Association and Institute of Materia Medica, Chinese Academy of Medical Sciences.

<https://doi.org/10.1016/j.apsb.2023.05.032>

2211-3835 © 2023 Chinese Pharmaceutical Association and Institute of Materia Medica, Chinese Academy of Medical Sciences. Production and hosting by Elsevier B.V. This is an open access article under the CC BY-NC-ND license (<http://creativecommons.org/licenses/by-nc-nd/4.0/>).

Inflammation;
Drug delivery;
Molecular mechanism

based microneedle patches combined with PC (PC@MLIP MN) was developed, which overcame the poor water solubility and weak skin permeability of PC, so that successfully punctured the skin and delivered PC to local tissues, and accurately regulated macrophage polarization in diabetic wound management. Overall, PC is an anti-inflammatory small molecule compound with a well-defined structure and dual-target regulation, and the PC@MLIP MN is a promising novel biomaterial for the management of diabetic wound.

© 2023 Chinese Pharmaceutical Association and Institute of Materia Medica, Chinese Academy of Medical Sciences. Production and hosting by Elsevier B.V. This is an open access article under the CC BY-NC-ND license (<http://creativecommons.org/licenses/by-nc-nd/4.0/>).

1. Introduction

Delayed wound healing in diabetes is a global challenge. In 2017, 79 billion US dollars were spent on treating diabetic diseases, including diabetic foot ulcers, in the United States alone¹. With the increasing prevalence of obesity and type 2 diabetes (T2DM), the impact of diabetic-delayed wound healing and expensive treatment will continue to rise². Therefore, the research and development of new drugs and strategies to promote diabetic wound healing are clinical problems that need to be solved urgently³. The wound-healing process involves complex molecular mechanisms, including inflammation, proliferation, and remodeling⁴. There have been extensive reports on the critical regulatory role of local macrophages in the early inflammation phase and their impact on the disorder and delay of diabetic wound healing⁴. In the normal wound healing process, inflammatory macrophages (M1 macrophages) are the main regulatory cells in the first few days (1–3 days) and then change to the M2 phenotype, which promotes tissue repair, healing, and regeneration. The overactivity of M1 macrophages leads to delayed wound healing in healthy and diabetic tissues⁵. The high-glucose microenvironment of diabetes promotes M1 macrophage activation and infiltration, which continuously infiltrates local tissues and releases inflammatory factors to prevent tissue repair, even in the late stage of wound healing⁶. Multiple studies have attempted to improve diabetic wound healing and have achieved significant treatment effects by regulating and inhibiting the function of local M1 macrophages^{7–9}. Therefore, the regulation of macrophage polarization is considered to be an essential strategy for treating diabetic wounds.

For decades, new drugs and materials regulating macrophage functions have been developed and studied, and natural products have played a significant role in drug discovery for centuries^{10,11}. Fungal metabolites are a major source of bioactive natural products¹². Bioprospecting fungal secondary metabolites in our laboratory have resulted in the discovery of a variety of novel bioactive compounds^{13–16}. One of the most promising discoveries was purpurolic acid (PC), a bergamotane sesquiterpene with a rare 6/4/5/5 tetracyclic ring system isolated from the fungus *Penicillium purpurogenum* IMM003^{15,17}. Members of this family have been isolated from diverse fungi, including purpurolic acids B–F^{15,17}, expansolides A–D¹⁸, decipenolides A and B¹⁹, sporulinalins A and B²⁰, donacinolides A and B²¹, and massarinolin A²². They have been reported to exhibit remarkable pancreatic lipase inhibitory^{15,17}, α -glucosidase inhibitory¹⁸, and antibacterial activities^{19,21,22}, and because of their unique structural features and drug potential, they have attracted significant interest from the researchers in chemistry, and the first elegant total synthesis of the

skeleton was accomplished by Wang and coworkers²³. It is worth noting that PC has never been reported to have anti-inflammatory activity in the field of inflammatory disease research. In this study, we found that PC showed significant anti-inflammatory activity and inhibited the activation of M1 macrophages without cytotoxicity, which showed the potential to regulate the function of local macrophages and promote wound healing in diabetes. Preliminary prediction of the physicochemical properties of PC revealed that PC fits well with Lipinski's 'Rule of Five' (Supporting Information Table S1)^{24,25}, indicating that PC might serve as a novel template for drug development. To investigate the anti-inflammation mechanism of PC, RNA-seq was performed to explore the regulatory pathway, and then various techniques including molecular docking calculations, SDS-PAGE, and surface plasmon resonance (SPR) detection were used to investigate the binding targets of PC. The results explained in detail that PC was a dual-target compound, which regulated macrophage activation by inhibiting both TLR4-MD2 dimerization and MYD88 phosphorylation. *Tlr4* knockout *in vivo* attenuated the promotion effect of PC on wound healing, which confirmed the *in vitro* conclusion. However, although the ideal method of wound healing administration is local application rather than systemic application, the calculated pharmacokinetic properties showed that the water solubility and skin permeability of PC were poor (Supporting Information Table S2 and Fig. S1), which limited the development and application of PC as a transdermal absorbent drug.

To overcome these weaknesses of PC, macrophage liposomes (MLIP) were loaded for both *in vivo* and *in vitro* anti-inflammatory treatments. Liposomes (LIP) are double-layer or multi-layer vesicles composed of phospholipids that can assemble DNA, small-molecule compounds, proteins, vaccines, and other substances through modification or loading methods to achieve efficient drug delivery²⁶. Simultaneously, liposomes are characterized by biological inertia, weak immunogenicity, low toxicity, and high biocompatibility. Thus, they are considered efficient and excellent drug carriers²⁷. Notably, liposomes prepared from the membranes of homologous cells show high homologous targeting *in vivo* owing to their specific membrane protein structure²⁸. Therefore, PC loaded with MLIP (PC@MLIP) achieved an accurate regulation on macrophages in this study. Microneedles (MNs) have recently attracted extensive research interest and have been widely used as drug delivery carriers *in vivo* wound healing research for drugs, including small molecule compounds, proteins, and cytokines²⁹. MNs are ideal drug delivery carriers for skin wounds because they minimize pain and tissue damage, overcome the difficulty of local drug delivery, and reduce the risk of wound exposure and infection³⁰. We hypothesized that liposomes can be

encapsulated in the tip of MNs, puncture the skin, and maintain an effective concentration of PC for a long time²⁹. And just as conjectured, PC@MLIP was loaded into Gelatin methacryloyl (GelMA)-based microneedles (PC@MLIP MN) to promote skin permeability, which successfully achieved the effect of diabetic wound healing promotion in type 2 diabetes (T2DM) mouse models.

In summary, we reported a small-molecule secondary metabolite of the endophytic fungus *Penicillium purpurogenum*, PC, showed the diabetic wound healing promotion effects by inhibiting inflammatory macrophage activation *via* inhibiting both TLR4-MD2 dimerization and MYD88 phosphorylation. Besides various techniques and *Tlr4* knockout mice to explore the targets of PC both *in vitro* and *in vivo*, macrophage liposomes and microneedles have been further used as carriers to improve the therapeutic efficacy of PC, providing a new strategy and basis for the application of small molecule compounds *in vivo*.

2. Materials and methods

2.1. Extraction and isolation of PC

See Supporting Information.

2.2. Isolation of mouse peritoneal macrophages

See Supporting Information.

2.3. *In vitro* induction and detections

See Supporting Information.

2.4. Preparation and characterization of PC@MLIP

Macrophage membranes were derived from RAW264.7 (China Infrastructure of Cell Line Resources, Beijing, China). Centrifugation (110000×g, 1 h, Beckman, Optima MAX-XP, CA, USA) and hypotonic treatments were applied to the cells to isolate the membranes. The separated macrophage cell membranes were hydrated with 10 mmol/L PC solution for 30 min and then loaded through repeated freezing–thawing cycles. Finally, a mini extruder (Avanti, 610000-1EA, Alabaster, AL, USA) was used to extrude the porous film of polycarbonate through 100 nm mesh to form the PC@MLIP. Dynamic light scattering (DLS, Zetasizer, NANO ZS, Marvin, UK) was used to analyze the hydrodynamic diameter and surface zeta potential of the PC@MLIP. Transmission electron microscopy (TEM, JEOL Co., Ltd., JEM-1400Flash, Tokyo, Japan) images were obtained to observe the PC@MLIP structure.

2.5. Preparation of PC@MLIP MN

50 μ L of GelMA solution containing 0.25% (g/mL) ultraviolet (UV) photoinitiator (EFL Co., Ltd., EFL-LAP, Suzhou, China) and PC@MLIP was used to prepare the PC@MLIP MN using a female polydimethylsiloxane (PDMS) mold. The patch was kept under vacuum for 10 min to remove air bubbles. Subsequently, another 50 μ L of GelMA solution containing ultraviolet (UV) photoinitiator was deposited to fill the needle cavities, followed by the removal of the excessive GelMA solution *via* a plastic scraper. We exposed the solution under 350 mW/cm² UV light (405 nm)

for 60 s. Then, the 5% (w/v) hyaluronic acid solution (EFL Co., Ltd.) was added to the composite base membrane. The PC@MLIP MN will be incubated at 30–35 °C for over 12 h before being detached from the PDMS mold.

2.6. Quantification analysis of PC in PC@MLIP

See Supporting Information.

2.7. Prediction of the physicochemical and ADME properties of PC

The prediction of the physicochemical and ADME properties of PC was performed using the website <http://biosig.unimelb.edu.au/pkcsmprediction> as reported³¹.

2.8. *In vivo* studies and detections

See Supporting Information. All experimental procedures were executed according to the protocols approved by the Animal Ethical and Welfare Committee of the Beijing Stomatological Hospital (KQYY-202206-007).

3. Results

3.1. PC inhibits LPS-induced M1 macrophage activation in both mouse peritoneal macrophages and RAW264.7 cells

PC was extracted according to the protocol reported in our previous study¹⁷, and its structure is shown in Fig. 1A. To explore the anti-inflammatory effect of PC, we isolated mouse peritoneal macrophages and investigated the regulatory effects of different concentrations of PC on LPS-induced M1 macrophage activation *in vitro*. Real-time PCR results showed that 1 μ mol/L PC significantly down-regulated LPS-induced *Nos2* gene expression, a marker of M1 macrophages (Fig. 1B)⁵. To further clarify this conclusion, western blotting was performed, and the results confirmed that 1 μ mol/L PC inhibited the expression of iNOS protein in LPS-induced macrophages (Fig. 1C and D). Immunohistochemical staining (Fig. 1E and G) and immunofluorescence staining (Fig. 1F and H) showed the down-regulation effect of PC on LPS-induced M1 macrophage activation by detecting the expression levels of M1 macrophage markers, iNOS and CD86. The flow cytometry analysis of CD80 and CD86 also confirmed the inhibition of PC on M1 macrophage activation (Fig. 1I and J). Moreover, for RAW264.7, PC also showed a significant inhibitory effect on M1 marker expression *in vitro* (Supporting Information Fig. S2A–S2D).

In addition, RNA sequencing (RNA-Seq) was used to assess changes in messenger RNA (mRNA) levels in mouse peritoneal macrophages cultured with PBS (control group), 1 μ g/mL LPS (LPS group) and 1 μ g/mL LPS + 1 μ mol/L PC (PC group). The heat map showed that PC intervention significantly reduced LPS-induced upregulation of various inflammatory factors, which further clarified the inhibitory effect of PC on inflammatory macrophage activation (Fig. 1K). Gene Set Enrichment Analysis (GSEA) showed that PC intervention induced the activation of drug metabolism process pathways, but significantly down-regulated the activation of the toll-like receptor signaling pathway and NF- κ B pathway compared with the LPS group (Fig. 1L). Since the TLR4-NF- κ B pathway is the classical signaling pathway during LPS-induced M1 macrophage activation³²,

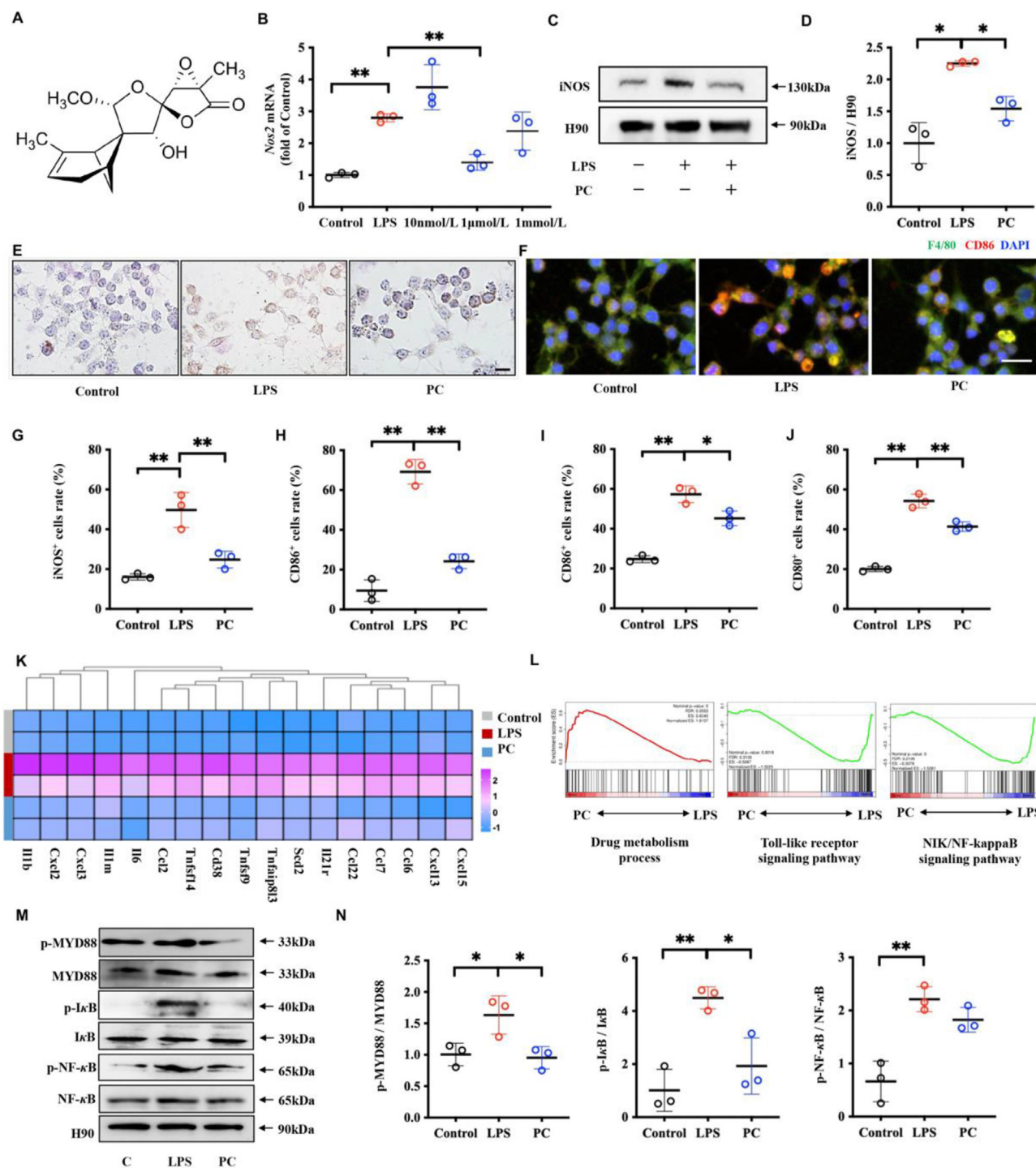


Figure 1 PC inhibits LPS-induced M1 macrophage activation in mouse peritoneal macrophages. (A) Structural formula of PC. (B) Real-time PCR results show that 1 $\mu\text{mol/L}$ PC inhibits the expression of *Nos2* in LPS-induced mouse peritoneal macrophages. (C, D) The results of western blotting observe a higher expression of iNOS protein in LPS-induced group, while 1 $\mu\text{mol/L}$ PC inhibits such up-regulation. (E, G) Immunohistochemical staining results show that 1 $\mu\text{mol/L}$ PC inhibits the ratio of iNOS⁺ macrophages induced by LPS. (F, H) The results of immunofluorescence staining confirm that 1 $\mu\text{mol/L}$ PC down-regulates LPS-induced CD86 expression, a marker of M1 macrophages. (I, J) Flow cytometry results show that LPS induces M1 macrophage polarization, resulting in an increase in the ratio of CD80⁺ and CD86⁺ cells, but 1 $\mu\text{mol/L}$ PC shows an inhibitory effect on this process. (K) The heat map shows that PC intervention significantly reduces the various inflammatory factors up-regulation induced by LPS in mouse peritoneal macrophages. (L) GSEA enrichment analysis between LPS group and PC group. (M, N) The results of western blotting indicate that PC inhibits LPS-induced NF- κ B pathway activation. All results are representative of at least three independent experiments. Scale bar in (E) and (F) = 10 μm . Data are presented as mean \pm SD ($n = 3$). * $P < 0.05$. ** $P < 0.01$.

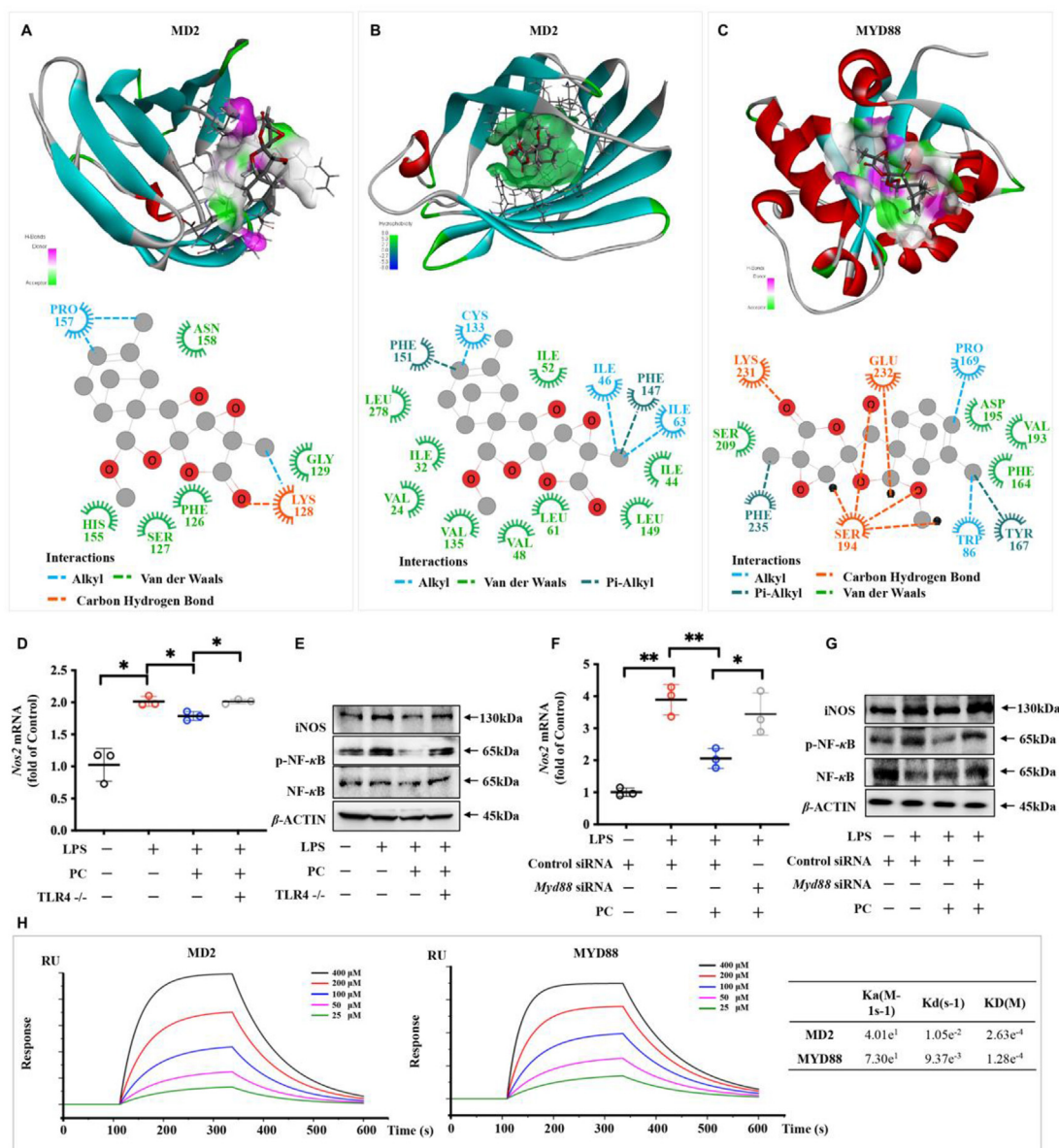


Figure 2 PC inhibits TLR4-NF- κ B pathway by binding with MD2 and MYD88 proteins. (A) The simulations of molecular docking demonstrate that PC can bind to the F126 loop of MD2, (B) and the hydrophobic LPS active site pocket of MD2. (C) PC can also bind to the BB loop of MYD88. (D, E) The regulatory effect of PC is obviously rescued when TLR4 is blocked in RAW264.7. (F, G) Similar, the inhibition effect of PC is reduced if MYD88 is blocked through *Myd88* siRNA transfection. (H) SPR detection of PC with MD2 protein and MYD88 protein. All results are representative of at least three independent experiments. Data are presented as mean \pm SD ($n = 3$). * $P < 0.05$. ** $P < 0.01$.

western blotting was performed to detect the expression levels of the NF- κ B pathway. The results showed that PC inhibited LPS-induced NF- κ B pathway activation (Fig. 1M and N), consistent with the RNA-Seq results. Therefore, these data indicate PC has a significant inhibitory effect on M1 macrophage activation in the inflammatory microenvironment, possibly through the TLR4-NF- κ B pathway.

3.2. PC inhibits M1 macrophage polarization by binding and inhibiting MD2 and MYD88 proteins

Next, molecular docking simulation was applied to explore whether all the key kinase proteins in the TLR4-NF- κ B pathway could dock with the PC structure to provide clues for the binding

targets of PC. The results demonstrated that PC could bind to F126 loop (Fig. 2A) and the hydrophobic LPS active site pocket of MD2 (Fig. 2B), blocking the binding of LPS to MD2 and the dimerization of TLR4^{33,34}. Furthermore, PC could also bind to the BB loop of MYD88 (Fig. 2C), which acted as a vital Toll/IL-1 receptor (TIR) domain, impairing TLR-induced cytokine induction³⁵. This is consistent with the previous *in vitro* results of PC inhibiting MYD88 phosphorylation (Fig. 1M). To prove these two target proteins of PC, TLR4 inhibitor and *Myd88* siRNA transfection were applied to knock out these corresponding genes in RAW264.7, respectively (Supporting Information Fig. S3). Real-time PCR and western blotting results confirmed that TLR4 (Fig. 2D and E) and MYD88 (Fig. 2F and G) were the key regulatory sites of PC, and when these sites were blocked, the

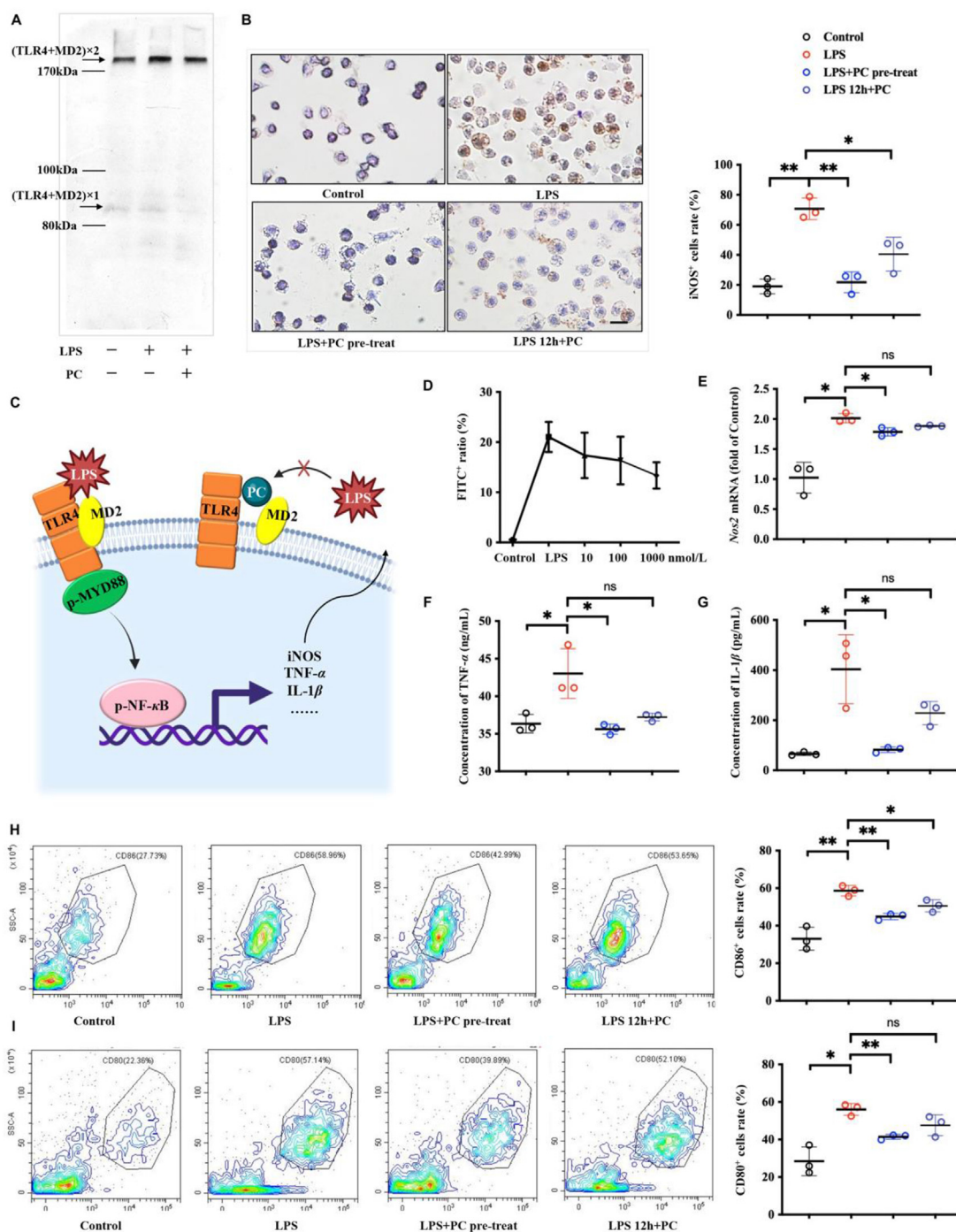


Figure 3 PC is a competitive antagonist of LPS by inhibiting TLR4-MD2 dimerization. (A) SDS-PAGE experiment explores the aggregation state of TLR4-MD2 in RAW264.7 after LPS binding. (B) The immunohistochemical staining results show that the inhibitory effect of PC pretreatment on LPS-induced iNOS expression is more significant compared with that of PC intervention 12 h after LPS induction. (C) Schematic illustration of the mechanism of PC antagonism against LPS. (D) Flow cytometry was applied to detect the FITC-LPS binding amount on the RAW264.7 cells after PC treatment. (E) The results of real-time PCR show that PC pretreatment has a more significant inhibitory effect on LPS-induced *Nos2* gene expression compared with that of PC intervention 12 h after LPS induction. (F,G) ELISA results show that PC pretreatment has a more significant inhibitory effect on the expression of inflammatory factors including TNF- α and IL-1 β compared with PC delayed treatment. (H,I) The antagonistic mechanism of PC against LPS is also validated through flow cytometry analysis of CD86 and CD80 expression, two M1 macrophage markers. All results are representative of at least three independent experiments. Scale bar in (B) = 10 μ m. Data are presented as mean \pm SD ($n = 3$). * $P < 0.05$. ** $P < 0.01$. ns, not significant. Figure created with BioRender.com.

regulatory effects of PC were rescued. More importantly, SPR detection confirmed the binding of PC with MD2 protein and MYD88 protein, with a binding power of 2.63×10^{-4} M and 1.28×10^{-4} M, respectively (Fig. 2H), which confirmed the results of our molecular docking. Therefore, these results indicate that PC inhibits M1 macrophage polarization by binding to and inhibiting MD2 and MYD88 proteins, thus inhibiting the activation of the downstream NF- κ B pathway.

3.3. PC is a competitive antagonist of LPS by inhibiting TLR4-MD2 dimerization

As one of the important membrane receptors on the surface of macrophages, TLR4 is the key receptor that binds LPS and responds quickly. However, TLR4 alone is not enough to recognize LPS, and the physical binding of TLR4 and MD2 is a prerequisite for ligand-induced activation³⁶. MD2 lacks transmembrane and intracellular regions and is related to the extracellular domain of TLR4, which is considered a component of the TLR4-MD2 complex and interacts with LPS^{33,34}. TLR4-MD2 dimerization induced by LPS is the starting point of downstream NF- κ B pathway activation and is also a key step in M1 macrophage polarization^{33,34}. Our molecular docking results indicated that PC has the potential to bind and inhibit the dimerization of TLR4-MD2. Moreover, this binding site coincided with the LPS induction site, suggesting that PC is an antagonist of LPS. To further characterize the structural and property changes of TLR4 polymer under PC intervention, SDS-PAGE was performed to explore the aggregation state of TLR4-MD2 in RAW264.7 after LPS binding (Fig. 3A). The results showed that the expression of the TLR4-MD2 dimer (molecular weight ~ 170 kDa) was increased after LPS induction, whereas this upregulation was inhibited by PC intervention, which proved the inhibitory effect of PC on the TLR4-MD2 dimer. As a result, the regulatory effect of PC delayed intervention (12 h after LPS induction) on macrophages is weaker than that of PC pretreatment (Fig. 3B), because one of the main regulatory mechanisms of PC is to competitively antagonize the target of LPS, thereby inhibiting downstream pathway activation (Fig. 3C). Flow cytometry was applied to detect the LPS binding amount on the RAW264.7 cells surface after induction by FITC-LPS, and the results showed that PC pretreatment significantly reduced the LPS binding amount in a dose-dependent manner (Fig. 3D), which confirmed the hypothesis. In addition, the antagonistic mechanism of PC against LPS was also validated through real-time PCR detection of *Nos2* gene expression (Fig. 3E), ELISA detection of inflammatory factors expression including TNF- α and IL-1 β (Fig. 3F and G), and flow cytometry analysis of M1 macrophage activation (Fig. 3H and I).

3.4. PC promotes wound healing by inhibiting M1 macrophage polarization via TLR4 pathway *in vivo*

In summary, our *in vitro* studies have shown that the TLR4 signaling pathway is the key pathway for PC to inhibit M1 macrophage polarization. PC achieves the effect of regulating macrophage function by inhibiting both the TLR4-MD2 dimerization and MYD88 phosphorylation, two targets of the TLR4 pathway. To demonstrate this regulation pathway of the PC *in vivo*, we established the skin wound healing model using wild-type (WT) or *Tlr4* gene knockout mice (*Tlr4*^{-/-}). Animals in PC groups were given 0.1 mL 10 μ mol/L PC injection once a day after establishment, and the animals in control group were given an equivalent

amount of PBS. After 7 days, we found that local injection of PC in WT mice significantly promoted the healing speed of skin wounds, whereas its therapeutic effect was reduced when *Tlr4* was knocked out *in vivo* (Fig. 4A–C). Immunohistochemical staining results showed that PC injection in WT mice significantly inhibited the ratio of local iNOS⁺ cells by the Day 3 after the injury, but this inhibitory effect disappeared when *Tlr4* was knocked out *in vivo* (Fig. 4D and E). Immunofluorescence staining for iNOS also showed a consistent trend (Supporting Information Fig. S6). ELISA was used to detect the expression levels of downstream inflammatory factors of M1 macrophages, and the results showed that PC injection down-regulated the levels of inflammatory factors including TNF- α and IL-1 β in WT mice, while *Tlr4* knockout *in vivo* attenuated these effects (Fig. 4F). Therefore, these results demonstrate that TLR4-related pathways play a key role in the PC regulation of M1 macrophage polarization.

3.5. Preparation and characterization of PC@MLIP MN

Despite the immune regulatory effect, the characteristics of poor water solubility and weak skin permeability determine that the *in vivo* application of PC can only be achieved by local injection rather than rubbing, which clearly limits the development of PC. Meanwhile, based on its regulation mechanism, accurate delivery strategies need to be developed to improve the treatment efficiency of PC. Therefore, we hypothesize that macrophage liposomes could be used to load PC to improve its water solubility and targeting effect, and microneedles (MNs) could be used as carriers to achieve long-term and effective local drug delivery. We hydrated the separated macrophage cell membrane with 10 mmol/L PC solution for 30 min according to the manufacturer's instructions and then loaded the compound through repeated freezing–thawing cycles. Finally, an Avanti mini extruder was used to extrude the porous film of polycarbonate (100 nm) to form PC@MLIP^{37,38}. Transmission electron microscopy (TEM) (Fig. 5A) and dynamic light scattering (DLS) (Fig. 5B) were used to determine the morphology and particle size of PC@MLIP. The results showed that the size distribution of PC@MLIP was uniform, which could reduce the difference in uptake efficiency caused by the uneven particle size distribution. Interestingly, although both showed negative electrical characteristics, the zeta potential of PC@MLIP was lower than that of empty MLIP (Fig. 5C). This might be caused by the unbalanced distribution of oxygen atoms in the structure and the presence of an electron-absorbing carbonyl group, which causes an uneven distribution of electrons and results in the overall electronegativity of the molecule. This result confirmed that in addition to being loaded inside the MLIP, PC also directly bound to TLR4 proteins on the surface of the MLIP. The quantification analysis of PC in PC@MLIP was performed by the ultra-high performance liquid chromatography coupled with triple quadrupole mass spectrometry (UPLC-QqQ-MS/MS) (Fig. 5D and Supporting Information Fig. S7), and the results showed that the loading efficiency (LE) of PC in PC@MLIP is $5.91 \pm 0.57\%$, w/w. Real-time PCR (Fig. 5E) and ELISA (Fig. 5F) results also indicated PC@MLIP showed the inhibition effect on LPS-induced inflammatory factors expression in RAW264.7, and this effect was dose-dependent (Fig. 5E). In addition, western blotting showed that PC@MLIP inhibited the activation of NF- κ B pathway induced by LPS in RAW264.7 (Supporting Information Fig. S8A). Moreover, immunofluorescence analysis showed that PC@MLIP inhibited the expression of the M1 macrophage marker CD86 (Fig. 5G) but did not affect the

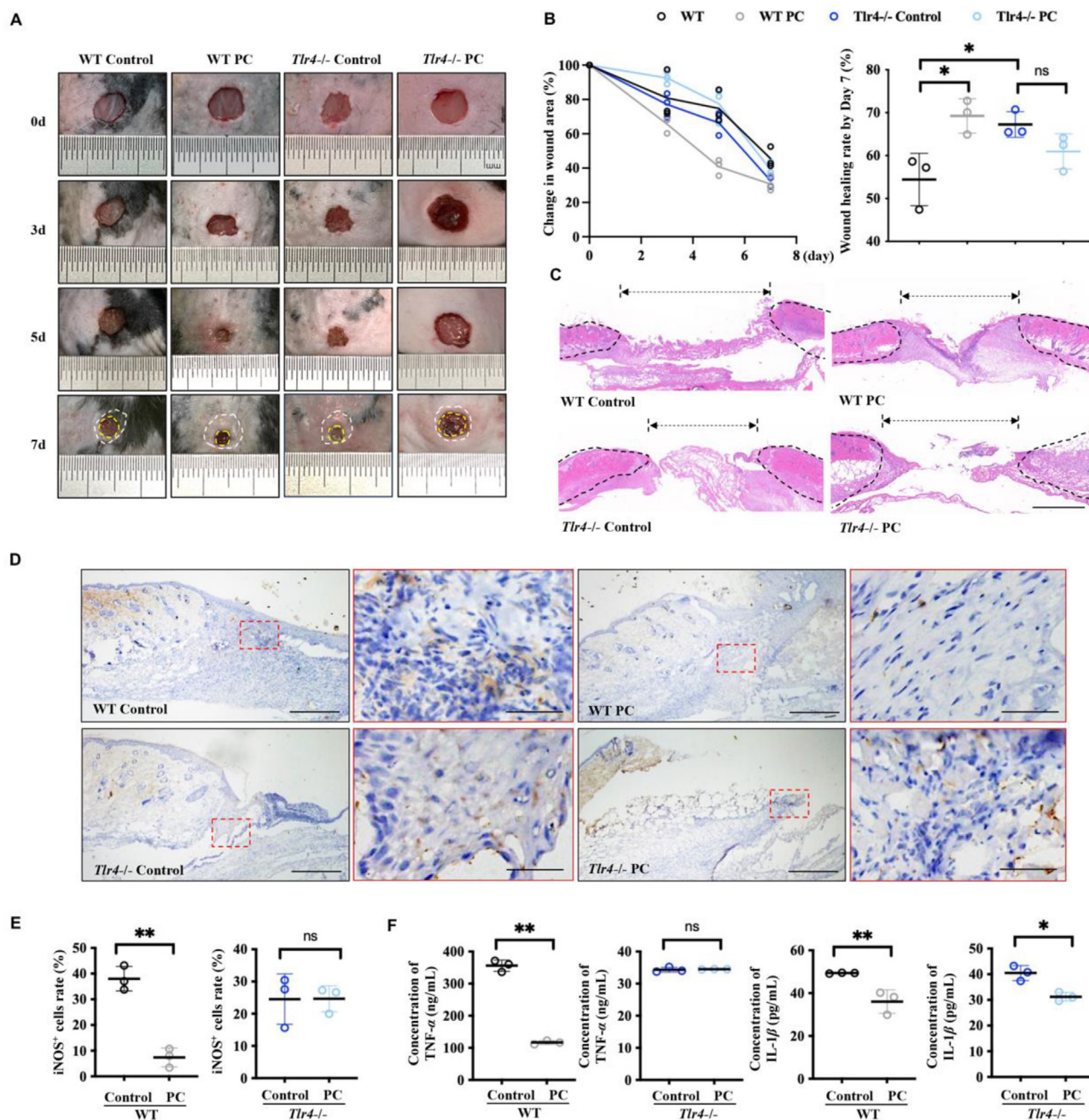


Figure 4 PC inhibits M1 macrophages activation through TLR4 pathway *in vivo*. (A, B) The wound healing promotion effect of PC is significantly reduced when *Tlr4* is knocked out *in vivo*. (C) H&E staining confirms that *Tlr4* knockout *in vivo* attenuates the promotion effect of PC on wound healing. (D, E) Immunohistochemical staining results indicate that PC injection in WT mice inhibits the ratio of local iNOS⁺ cells by the Day 3 after the injury, but this inhibitory effect disappears when *Tlr4* is knocked out *in vivo*. (F) ELISA results show that PC injection significantly down-regulates the level of inflammatory factors including TNF- α and IL-1 β in WT mice, while *Tlr4* knockout *in vivo* attenuates these effects. All results are representative of at least three independent experiments. Scale bar in (C) = 1 mm. Scale bar in (D) = 500 μ m in low power visual field and 50 μ m in high power visual field. Data are presented as mean \pm SD ($n = 3$). * $P < 0.05$. ** $P < 0.01$. ns, not significant.

activity of the cells (Fig. 5H). All these results indicate that PC@MLIP has characteristics similar to PC in regulating macrophage polarization. However, whether PC@MLIP also has the advantage of homologous targeting that MLIP should bring about remains to be verified. By adding PC@MLIP (PKH26 labeled, red) into the co-culture system composed of human

umbilical vein endothelial cells (HUVECs) (PKH67 labeled, green) and RAW264.7 (unlabeled), we found that PC@MLIP co-localized with most macrophages 6 h later, which confirmed the good homologous targeting characteristics of PC@MLIP (Fig. 5I). Therefore, we believe that PC@MLIP can accurately deliver to and regulate the macrophage activation.

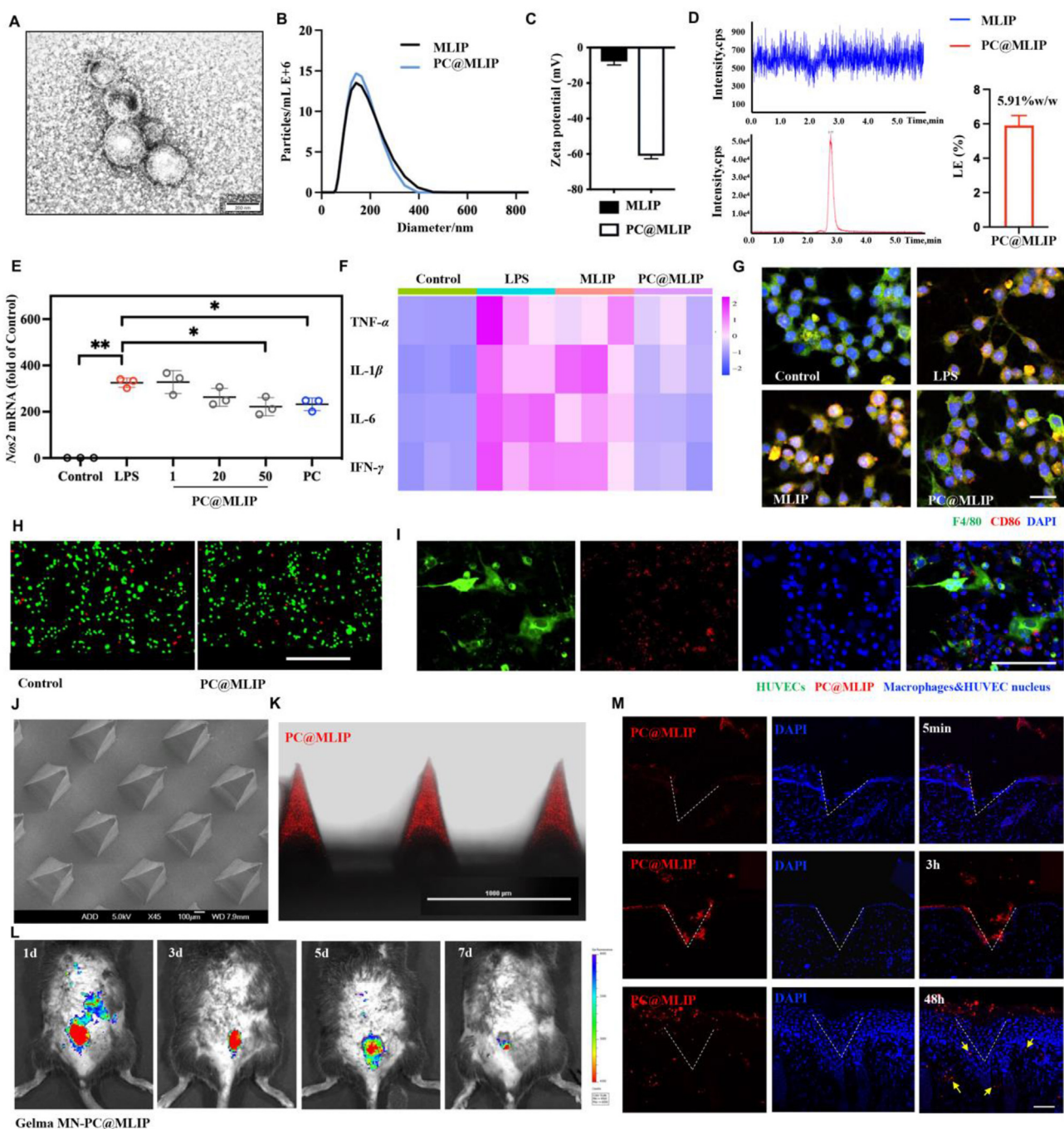


Figure 5 PC@MLIP MN design and preparation. (A) TEM of PC@MLIP. (B) There is no significant change in the particle size of PC@MLIP compared with MLIP. (C) Zeta potential analysis results of MLIP and PC@MLIP. (D) The UPLC-MS/MS chromatogram of MLIP (blue line) and PC@MLIP (red line), and the loading efficiency (LE) of PC in PC@MLIP is $5.91 \pm 0.57\%$, w/w. (E) PC@MLIP (1, 20, and 50 μg) shows a dose-dependent inhibition effect on LPS-induced *Nos2* gene expression levels in RAW264.7. (F) PC@MLIP down-regulates multiple inflammatory factors expression in RAW264.7. (G) Immunofluorescence shows that PC@MLIP reduces the ratio of CD86⁺ RAW264.7 cells. (H) Live/Dead results indicate PC@MLIP shows no cytotoxicity. (I) The good homologous targeting characteristics of PC@MLIP are confirmed by adding PC@MLIP (PKH26 labeled, red) into the co-culture system composed of HUVECs (PKH67 labeled, green) and RAW264.7 (unlabeled). (J) SEM image of PC@MLIP MN. (K) The confocal result shows the PC@MLIP (Cy7se marked, red) position at the tip of the microneedles. (L) The *in vivo* fluorescence imaging results show that local PC release can be maintained for up to 5 days after the PC@MLIP MN administration. (M) The baseline results after 5 min of PC@MLIP MN administration show that there is no vesicle release at this time. After 3 h of administration, the vesicles have been released and positioned on the skin surface. After 48 h of administration, the released vesicles have been delivered to the deep tissue. All results are representative of at least three independent experiments. Scale bar in (G) = 10 μm . Scale bar in (H) and (I) = 100 μm . Scale bar in (M) = 50 μm . Data are presented as mean \pm SD ($n = 3$). * $P < 0.05$. ** $P < 0.01$. ns, not significant.

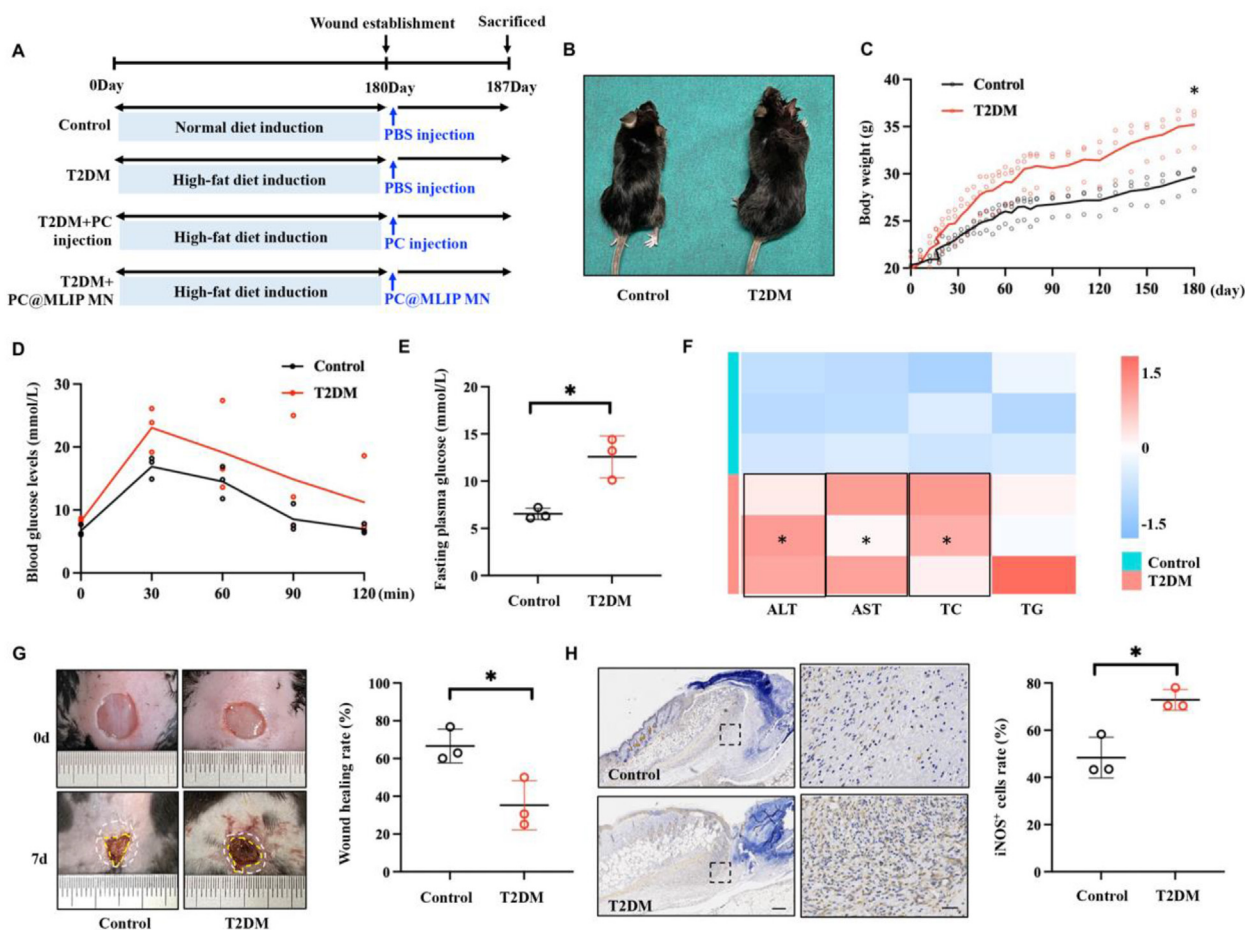


Figure 6 Establishment of T2DM mice wound healing models. (A) Schematic illustration of the establishment of T2DM model and the intervention timing in the process of wound healing. (B, C) At the end point of the T2DM model establishment, the weights of T2DM mice (T2DM group) increase significantly compared with healthy mice (control group). (D, E) Glucose tolerance curve and fasting glucose results in control group and T2DM group. (F) The blood biochemical results of T2DM mice show an overexpression trend compared with those of healthy mice. (G) The wound healing speed of T2DM mice is significantly slower by the Day 7 after surgery. (H) Immunohistochemical staining results show that iNOS⁺ M1 macrophages were overactivated at the early stage of wound healing in T2DM mice. All results are representative of at least three independent experiments. Scale bar in (H) = 200 μ m in low power visual field and 30 μ m in high power visual field. Data are presented as mean \pm SD ($n = 3$). * $P < 0.05$.

Besides, MN patch was selected as the carrier for drug delivery *in vivo* because of its permeability and sustained-release characteristics. In this study, GelMA hydrogel was used as the preparation material for MN patch owing to its good biocompatibility³⁹. We added PC@MLIP during the preparation of MN patch, settled the vesicles at the tip of the MNs, and then further cross-linked to form the PC@MLIP MN, which was a 12.4 mm \times 12.4 mm, 10 \times 10 array patch. Each MN had an 800 μ m high standard pyramid geometry, with a 5 μ m tip diameter and 320 μ m bottom diameter, as confirmed by scanning electron microscopy (SEM) (Fig. 5J). The confocal microscopy results clearly showed the PC@MLIP (Cy7se marked, red) position at the tip of the micro-needles (Fig. 5K). By placing PC@MLIP MN in 50% fetal bovine serum (FBS)⁴⁰ and continuously monitoring the released protein concentration in the supernatant, we found that PC@MLIP MN released the vesicles smoothly in FBS, which could last for up to a week (Fig. S8B). The *in vivo* fluorescence imaging results showed that owing to the sustained release characteristics of GelMA MNs, the local PC release could be maintained for up to 5 days after the PC@MLIP MN was inserted into the skin (Fig. 5L). This

regulation duration fully covered the early inflammation phase of M1 macrophage activation and infiltration, thereby ensuring the timely and continuous delivery of drugs to the subcutaneous connective tissue with minimal injury. Fig. 5M shows the local vesicle release situation after PC@MLIP MN administration. The baseline results after 5 min of administration show that there is no vesicle release at this time. After 3 h of administration, the vesicles have been released and positioned on the skin surface. After 48 h of administration, the released vesicles have been delivered to the deep tissue. In summary, the combination of liposomes and microneedles enables the effective delivery and long-term concentration maintenance of PC, making it an ideal candidate for the management of diabetic wounds.

3.6. PC@MLIP MN significantly promotes diabetic wound healing speed *in vivo*

Based on a previous study⁴¹, we established a mouse T2DM model by high-fat diet (HFD) induction (Fig. 6A). The successful establishment of the T2DM model was confirmed by the results of

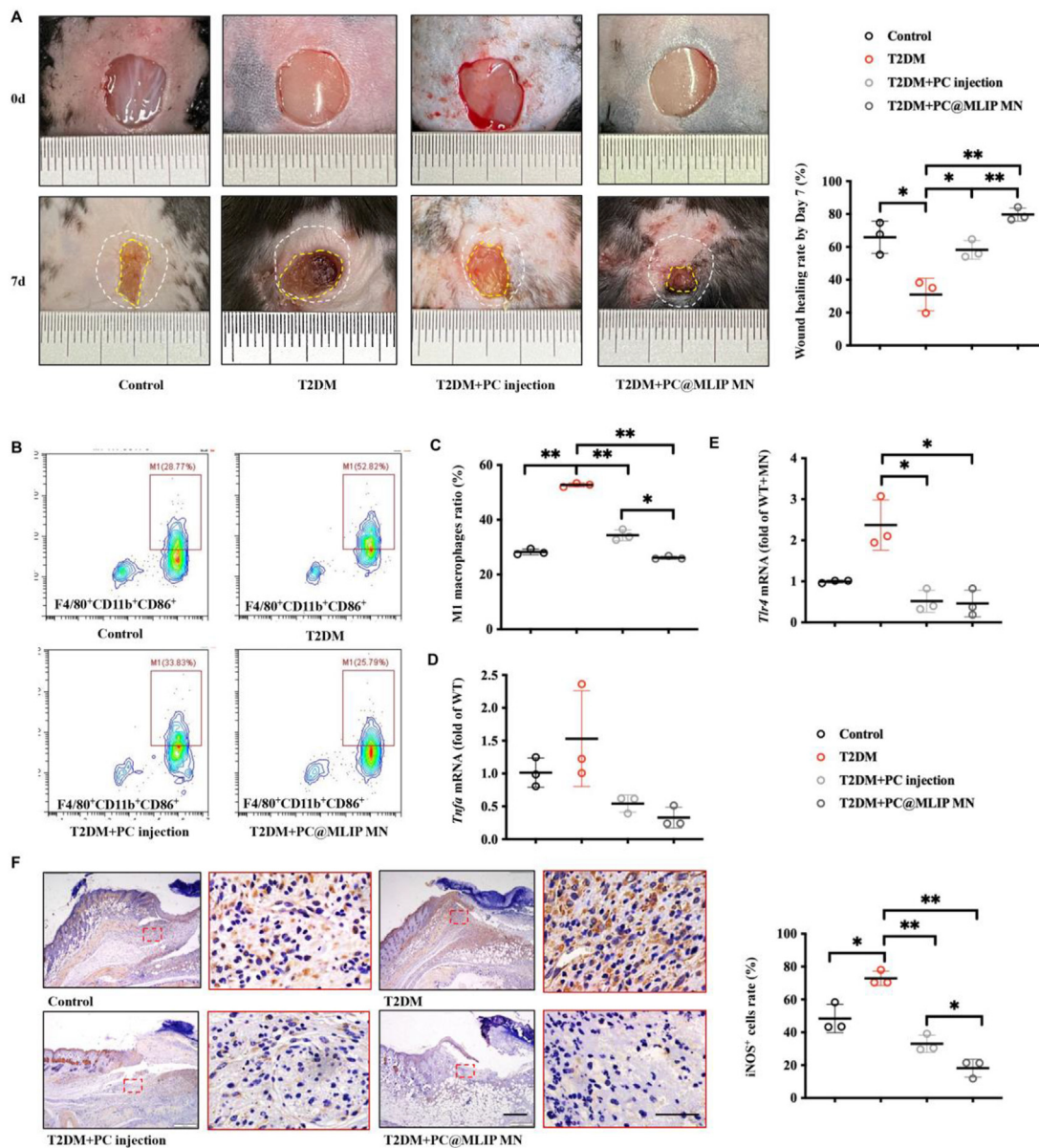


Figure 7 PC@MLIP MN promotes diabetic wound healing through targeted and long-acting inhibition of local M1 macrophages. (A) PC@MLIP MN significantly promotes diabetic wound healing speed, and its therapeutic effect is better than that of PC injection. (B, C) Flow cytometry confirms that PC@MLIP MN reduces the infiltration of M1 macrophages *in vivo*. (D) Real-time PCR results show that PC@MLIP MN application reduces the gene expression of local *Tnfa*. (E) Both PC injection and PC@MLIP MN application reduce the gene expression of *Tlr4*. (F) Immunohistochemical staining results of local iNOS⁺ cells by the Day 3 after injury reflect the advantages of the accurate regulation effect of PC@MLIP. All results are representative of at least three independent experiments. Scale bar in (F) = 500 μ m in low power visual field and 50 μ m in high power visual field. Data are presented as mean \pm SD ($n = 3$). * $P < 0.05$. ** $P < 0.01$.

body weight (Fig. 6B and C), blood glucose (Fig. 6D and E), and blood biochemical detections (Fig. 6F). By establishing a round wound with a diameter of 1 cm on the back skin of healthy mice (control group) and T2DM mice (T2DM group) (Fig. 6A), we found that the wound healing speed of T2DM mice was significantly slower by the Day 7 after surgery (Fig. 6G and Supporting Information Fig. S9B), and the local M1 macrophages were over-activated, with high expression of multiple inflammatory factors in wound tissues (Fig. 6H and Fig. S9C–S9H), which was consistent with previous results⁴². *In vivo* knockout of *Tlr4* rescued the wound healing delay (Fig. S9I–S9J), which confirmed that over-

activation of local M1 macrophages is a key factor in wound healing difficulty in T2DM mice.

After confirming the successful preparation of the PC@MLIP MN and its theoretical possibility of promoting wound healing, we used healthy mice and T2DM mice to establish the wound healing models and administered PBS injection (control group and T2DM group), PC injection (T2DM + PC injection group), and PC@MLIP MN (T2DM + PC@MLIP MN group) to each group immediately after surgery. By the Day 7 after establishment, we found that PC@MLIP MN significantly promoted diabetic wound healing speed, and its therapeutic effect was better than that of PC

injection (Fig. 7A). Flow cytometry (Fig. 7B) was used to determine the ratio of local M1 macrophages ($F4/80^+CD11b^+CD86^+$) in the wound tissue of T2DM mice, and the results confirmed that PC@MLIP MN reduced the infiltration of M1 macrophages (Fig. 7C). Real-time PCR results also showed that the PC@MLIP MN application reduced the gene expression of local *Tnfa* (Fig. 7D). Interestingly, both PC injection and PC@MLIP MN application reduced the gene expression of *Tlr4* with no significant differences (Fig. 7E). However, the differences between the regulatory effect on local $iNOS^+$ macrophages (Fig. 7F) and the therapeutic effect on diabetic wound healing reflected the advantages of the accurate regulation effect of PC@MLIP. These results further illustrated that the PC@MLIP MN is an ideal material for promoting diabetic wound healing.

In summary, through the assembly of PC and MLIP, we achieved PC loading on the surface and inside the MLIP and further achieved continuous drug release at the early stage of healing by settling PC@MLIP at the tip of the GelMA-based MNs. The released vesicles tend to be delivered to local macrophages because of their homologous targeting characteristics and reduce the activation of M1 macrophages by inhibiting the membrane receptor TLR4. Meanwhile, even if macrophages phagocytosed PC@MLIP, the released PC could bind MYD88 protein internally and inhibit its activity, thereby achieving an efficient and accurate regulatory effect. The slow-release characteristics of GelMA-based MN ensure the long-term concentration maintenance of PC in wound tissues during the critical early stage of M1 macrophage activation, thus achieving significant therapeutic effect on diabetic wound healing promotion (Fig. 8).

4. Discussion

To date, it has been reached a consensus that obesity-related diseases including T2DM and hypertension are closely related to chronic inflammation^{43,44}. Immune cells are the main effectors of the local inflammatory response, and macrophages show significant phenotypic heterogeneity in diabetes tissues. Multiple reports have confirmed that monocytes recruited in T2DM tissue would differentiate into M1-type macrophages, whose excessive accumulation leads to the imbalance between M1/M2 macrophages⁴⁵. The inflammatory factors and cell signals produced by M1 macrophages will enhance local inflammation and promote tissue

destruction⁴⁶, even further damaging the host's glucose tolerance⁴⁵. Since T2DM is considered to be a costly disease, of which nearly one-third of the cost is attributable to the treatment of diabetic foot disease, including chronic and unhealed diabetic wounds¹, many studies have invested a lot of energy to explore the pathogenesis and treatments of diabetic wounds healing delay. Some studies have reported the key role of TLR4/NF- κ B signaling pathway⁴⁷, and tried to promote T2DM wound repair by inhibiting the polarization of local M1 macrophages^{48–50}. Although a variety of natural products and small molecule compounds have been developed to regulate the macrophage activation and functions, multiple limitations including low water solubility, low targeting and weak skin permeability need to be overcome, which greatly compromise the therapeutic effect of drugs *in vivo*.

In this study, a promising small-molecule secondary metabolite of the endophytic fungus *Penicillium purpurogenum*, PC, was reported to show the diabetic wound healing promotion effects by inhibiting inflammatory macrophage activation. Based on the results of RNA-seq, we found that NF- κ B pathway plays a key role during the PC regulation. Therefore, we focused on the key protein targets in this pathway and conducted a detailed exploration using molecular docking calculations, SDS-PAGE, and SPR detection, and ultimately demonstrated that PC inhibits the NF- κ B pathway by inhibiting TLR4-MD2 dimerization and inhibiting the phosphorylation of MYD88, which is crucial for regulating local macrophage polarization to promote wound healing in diabetes. Moreover, PC-based targeted immune regulatory microneedle, PC@MLIP MN, was developed. PC@MLIP MN consisted of PC, macrophage membrane liposome MLIP, and GelMA-based microneedles. MLIP showed homologous targeting characteristics and improved the water solubility of PC. GelMA-based MNs could achieve continuous drug release and promote its skin permeability. Therefore, PC@MLIP MN addressed the lack of PC including poor water solubility and weak skin permeability, and improved its treatment efficiency by accurately regulating local macrophage functions. *In vivo* studies indicated that PC@MLIP MN could release PC continuously in the early stage of injury, and promote diabetic wound healing by accurately inhibiting local M1 macrophage activation. The remarkable promoting effect on diabetic wound healing proves the rationality and effectiveness of the PC@MLIP MN design.

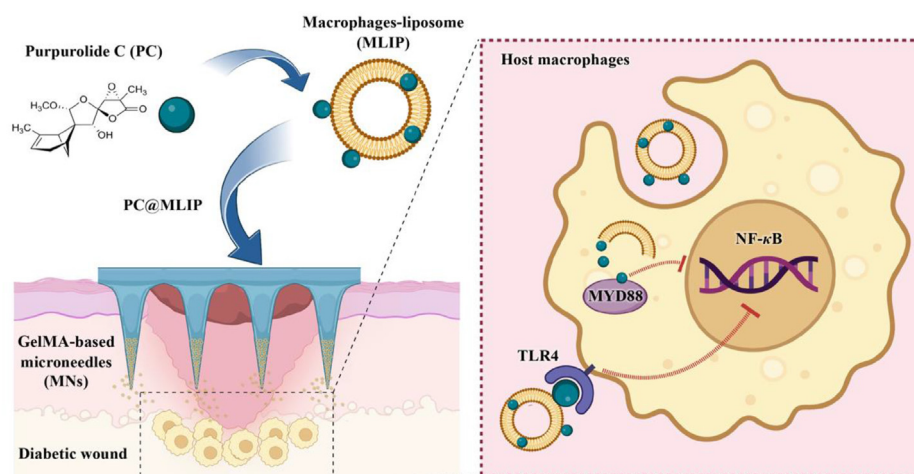


Figure 8 Schematic illustration of regulation mechanism of PC@MLIP MN in diabetic wound tissues. Figure created with [BioRender.com](https://www.biorender.com).

5. Conclusions

As an innovative small molecule compound for tissue healing promotion, PC has shown multiple advantages, including mature purification process and clear mechanism targets. The design of PC@MLIP MN ingeniously address its shortcomings, achieving efficient drug delivery, accurate macrophage regulatory effect, ideal mechanical strength and good biocompatibility. Overall, the PC@MLIP MN is promising as a new material for the management of diabetic wounds, and also provides a new strategy and basis for the application of small molecule compounds *in vivo*.

Acknowledgments

This work was supported by grants from National Key R&D Program of China (Grant NO. 2022YFC2504200 to Yi Liu), the National Nature Science Foundation of China (81991504 and 81974149 to Yi Liu, 82073978 to Sheng Lin, 82201053 to Yitong Liu, 81803397 to Guiyang Xia, 82122015 to Junji Xu), the Innovation Research Team Project of Beijing Stomatological Hospital, Capital Medical University (CXTD202202 to Yi Liu, China), the Innovation Foundation of Beijing Stomatological Hospital, Capital Medical University (21-09-18 to Lijia Guo, China), the Beijing Stomatological Hospital, Capital Medical University Young Scientist Program (YSP202105 to Yitong Liu, China), the Beijing Municipal Administration of Hospitals Clinical Medicine Development of Special Funding Support (ZYLX202121 to Yi Liu, China), Beijing Municipal Administration of Hospitals' Ascent Plan (DFL20181501 to Yi Liu, China), Beijing Municipal Administration of Hospitals' Youth Programme (QML20181501 to Lijia Guo, QML20231506 to Yitong Liu, China), Beijing Municipal Administration of Hospitals Incubating Program (PX2023054 to Lijia Guo, China).

Author contributions

Yitong Liu designed, conducted, and supervised the anti-inflammation evaluation of the material in this study, and contributed to the manuscript preparation. Guiyang Xia isolated the compound and elucidated its structure, and contributed to the quantification analysis. Yingyi Chen performed the majority of the schematic figures with the aid of Huan Xia and Junji Xu. Lijia Guo designed the *in vivo* study and wrote the manuscript. Sheng Lin designed the compound isolation and material preparation, and wrote the manuscript. Yi Liu designed the *in vitro* study and wrote the manuscript. All authors contributed to the article and approved the submitted version.

Conflicts of interest

The authors have no conflicts of interest to declare.

Appendix A. Supporting information

Supporting data to this article can be found online at <https://doi.org/10.1016/j.apsb.2023.05.032>.

References

- Louiselle AE, Niemiec SM, Zgheib C, Liechty KW. Macrophage polarization and diabetic wound healing. *Transl Res* 2021;**236**:109–16.
- Han G, Ceilley R. Chronic wound healing: a review of current management and treatments. *Adv Ther* 2017;**34**:599–610.
- Wu H, Yang P, Li A, Jin X, Zhang Z, Lv H. *Chlorella* sp.-ameliorated undesirable microenvironment promotes diabetic wound healing. *Acta Pharm Sin B* 2023;**13**:410–24.
- Qian Y, Zheng Y, Jin J, Wu X, Xu K, Dai M, et al. Immunoregulation in diabetic wound repair with a photoenhanced glycyrrhizic acid hydrogel scaffold. *Adv Mater* 2022;**34**:e2200521.
- Xia H, Liu Y, Xia G, Liu Y, Lin S, Guo L. Novel isoquinoline alkaloid litcubanin a – a potential anti-inflammatory candidate. *Front Immunol* 2021;**12**:685556.
- Liechty C, Hu J, Zhang L, Liechty KW, Xu J. Role of microRNA-21 and its underlying mechanisms in inflammatory responses in diabetic wounds. *Int J Mol Sci* 2020;**21**:3328.
- Zeng X, Chen B, Wang L, Sun Y, Jin Z, Liu X, et al. Chitosan@Puerarin hydrogel for accelerated wound healing in diabetic subjects by miR-29ab1 mediated inflammatory axis suppression. *Bioact Mater* 2023;**19**:653–65.
- Yang H, Song L, Sun B, Chu D, Yang L, Li M, et al. Modulation of macrophages by a paeoniflorin-loaded hyaluronic acid-based hydrogel promotes diabetic wound healing. *Mater Today Bio* 2021;**12**:100139.
- Mirza RE, Fang MM, Ennis WJ, Koh TJ. Blocking interleukin-1beta induces a healing-associated wound macrophage phenotype and improves healing in type 2 diabetes. *Diabetes* 2013;**62**:2579–87.
- Newman DJ, Cragg GM. Natural products as sources of new drugs over the nearly four decades from 01/1981 to 09/2019. *J Nat Prod* 2020;**83**:770–803.
- Zhi K, Wang J, Zhao H, Yang X. Self-assembled small molecule natural product gel for drug delivery: a breakthrough in new application of small molecule natural products. *Acta Pharm Sin B* 2020;**10**:913–27.
- Schueffler A, Anke T. Fungal natural products in research and development. *Nat Prod Rep* 2014;**31**:1425–48.
- Wu YZ, Zhang HW, Sun ZH, Dai JG, Hu YC, Li R, et al. Bysspectin A, an unusual octaketide dimer and the precursor derivatives from the endophytic fungus *Byssoschlamys spectabilis* IMM002 and their biological activities. *Eur J Med Chem* 2018;**145**:717–25.
- Wu YZ, Xia GY, Xia H, Wang LY, Wang YN, Li L, et al. Seco and nor-seco isodihilarane-type meroterpenoids from *Penicillium purpurogenum* and the configuration revisions of related compounds. *J Nat Prod* 2022;**85**:248–55.
- Xia GY, Wang LY, Zhang JF, Wu YZ, Ge GB, Wang YN, et al. Three new polyoxygenated bergamotanes from the endophytic fungus *Penicillium purpurogenum* IMM 003 and their inhibitory activity against pancreatic lipase. *Chin J Nat Med* 2020;**18**:75–80.
- Lin S, Wu YZ, Chen KY, Ye J, Yang XW, Zhang WD. Polyketides from the fungus *Penicillium decumbens*. *J Asian Nat Prod Res* 2018;**20**:445–50.
- Wang YN, Xia GY, Wang LY, Ge GB, Zhang HW, Zhang JF, et al. Purpurolide A, 5/5/5 spirocyclic sesquiterpene lactone in nature from the endophytic fungus *Penicillium purpurogenum*. *Org Lett* 2018;**20**:7341–4.
- Ying YM, Fang CA, Yao FQ, Yu Y, Shen Y, Hou ZN, et al. Bergamotane sesquiterpenes with alpha-glucosidase inhibitory activity from the plant pathogenic fungus *Penicillium expansum*. *Chem Biodivers* 2017;**14**:e1600184.
- Che Y, Gloer JB, Koster B, Malloch D. Decipinin A and decipeniolides A and B: new bioactive metabolites from the coprophilous fungus *Podospira decipiens*. *J Nat Prod* 2002;**65**:916–9.
- Zhang LH, Feng BM, Chen G, Li SG, Sun Y, Wu HH, et al. Sporulaminals A and B: a pair of unusual epimeric spiroaminal derivatives from a marine-derived fungus *Paraconiothyrium sporulosum* YK-03. *RSC Adv* 2016;**6**:42361–6.
- Zhao ZZ, Zhao K, Chen HP, Bai X, Zhang L, Liu JK. Terpenoids from the mushroom-associated fungus *Montagnula donacina*. *Phytochemistry* 2018;**147**:21–9.
- Oh H, Gloer JB, Shearer CA, Massarinos A–C. New bioactive sesquiterpenoids from the aquatic fungus *Massarina tunicata*. *J Nat Prod* 1999;**62**:497–501.

23. Wang YC, Cui C, Dai M. Flow chemistry-enabled divergent and enantioselective total syntheses of massarinolin A, purpurosides B, D, E, 2,3-deoxypurpurosides C, and structural revision of massarinolin A. *Angew Chem Int Ed Engl* 2021;**60**:24828–32.
24. Lipinski CA, Lombardo F, Dominy BW, Feeney PJ. Experimental and computational approaches to estimate solubility and permeability in drug discovery and development settings. *Adv Drug Deliv Rev* 2001;**46**:3–26.
25. Lipinski CA. Lead- and drug-like compounds: the rule-of-five revolution. *Drug Discov Today Technol* 2004;**1**:337–41.
26. Rideau E, Dimova R, Schwille P, Wurm FR, Landfester K. Liposomes and polymersomes: a comparative review towards cell mimicking. *Chem Soc Rev* 2018;**47**:8572–610.
27. Gulbake A, Jain A, Jain A, Jain SK. Insight to drug delivery aspects for colorectal cancer. *World J Gastroenterol* 2016;**22**:582–99.
28. Li J, Zeng H, You Y, Wang R, Tan T, Wang W, et al. Active targeting of orthotopic glioma using biomimetic liposomes co-loaded elemene and cabazitaxel modified by transferritin. *J Nanobiotechnol* 2021;**19**:289.
29. Yin M, Wu J, Deng M, Wang P, Ji G, Wang M, et al. Multifunctional magnesium organic framework-based microneedle patch for accelerating diabetic wound healing. *ACS Nano* 2021;**15**:17842–53.
30. Ahmed Saeed Al-Japirai K, Mahmood S, Hamed Almurisi S, Reddy Venugopal J, Rebhi Hilles A, Azmana M, et al. Current trends in polymer microneedle for transdermal drug delivery. *Int J Pharm* 2020;**587**:119673.
31. Pires DE, Blundell TL, Ascher DB. pkCSM: predicting small-molecule pharmacokinetic and toxicity properties using graph-based signatures. *J Med Chem* 2015;**58**:4066–72.
32. Ye Y, Wang Y, Yang Y, Tao L. Aloperine suppresses LPS-induced macrophage activation through inhibiting the TLR4/NF-kappaB pathway. *Inflamm Res* 2020;**69**:375–83.
33. Kim HM, Park BS, Kim JI, Kim SE, Lee J, Oh SC, et al. Crystal structure of the TLR4-MD-2 complex with bound endotoxin antagonist Eritoran. *Cell* 2007;**130**:906–17.
34. Park BS, Song DH, Kim HM, Choi BS, Lee H, Lee JO. The structural basis of lipopolysaccharide recognition by the TLR4-MD-2 complex. *Nature* 2009;**458**:1191–5.
35. Snyder GA, Cirl C, Jiang J, Chen K, Waldhuber A, Smith P, et al. Molecular mechanisms for the subversion of MyD88 signaling by TcpC from virulent uropathogenic Escherichia coli. *Proc Natl Acad Sci U S A* 2013;**110**:6985–90.
36. Nagai Y, Akashi S, Nagafuku M, Ogata M, Iwakura Y, Akira S, et al. Essential role of MD-2 in LPS responsiveness and TLR4 distribution. *Nat Immunol* 2002;**3**:667–72.
37. Luk BT, Hu CM, Fang RH, Dehaini D, Carpenter C, Gao W, et al. Interfacial interactions between natural RBC membranes and synthetic polymeric nanoparticles. *Nanoscale* 2014;**6**:2730–7.
38. Li T, Mudie S, Cipolla D, Rades T, Boyd BJ. Solid state characterization of ciprofloxacin liposome nanocrystals. *Mol Pharm* 2019;**16**:184–94.
39. Liu Y, Long L, Zhang F, Hu X, Zhang J, Hu C, et al. Microneedle-mediated vascular endothelial growth factor delivery promotes angiogenesis and functional recovery after stroke. *J Cont Release* 2021;**338**:610–22.
40. Thamphiwatana S, Angsantikul P, Escajadillo T, Zhang Q, Olson J, Luk BT, et al. Macrophage-like nanoparticles concurrently absorbing endotoxins and proinflammatory cytokines for sepsis management. *Proc Natl Acad Sci U S A* 2017;**114**:11488–93.
41. Xu Y, Van Hul M, Suriano F, Preat V, Cani PD, Beloqui A. Novel strategy for oral peptide delivery in incretin-based diabetes treatment. *Gut* 2020;**69**:911–9.
42. Kominato H, Takeda K, Mizutani K, Mikami R, Kido D, Buranasin P, et al. Metformin accelerates wound healing by Akt phosphorylation of gingival fibroblasts in insulin-resistant prediabetes mice. *J Periodontol* 2022;**93**:256–68.
43. Noto H, Goto A, Tsujimoto T, Osame K, Noda M. Latest insights into the risk of cancer in diabetes. *J Diabetes Investig* 2013;**4**:225–32.
44. Osborn O, Olefsky JM. The cellular and signaling networks linking the immune system and metabolism in disease. *Nat Med* 2012;**18**:363–74.
45. Kraakman MJ, Murphy AJ, Jandeleit-Dahm K, Kammoun HL. Macrophage polarization in obesity and type 2 diabetes: weighing down our understanding of macrophage function?. *Front Immunol* 2014;**5**:470.
46. Sun Z, Liu Q, Lv Z, Li J, Xu X, Sun H, et al. Targeting macrophagic SHP2 for ameliorating osteoarthritis via TLR signaling. *Acta Pharm Sin B* 2022;**12**:3073–84.
47. Ti D, Hao H, Tong C, Liu J, Dong L, Zheng J, et al. LPS-preconditioned mesenchymal stromal cells modify macrophage polarization for resolution of chronic inflammation via exosome-shuttled let-7b. *J Transl Med* 2015;**13**:308.
48. Zhang X, Dai J, Li L, Chen H, Chai Y. NLRP3 inflammasome expression and signaling in human diabetic wounds and in high glucose induced macrophages. *J Diabetes Res* 2017;**2017**:5281358.
49. Kim SY, Nair MG. Macrophages in wound healing: activation and plasticity. *Immunol Cell Biol* 2019;**97**:258–67.
50. Wang Q, Zhu G, Cao X, Dong J, Song F, Niu Y. Blocking AGE-RAGE signaling improved functional disorders of macrophages in diabetic wound. *J Diabetes Res* 2017;**2017**:1428537.